Supporting Information

Alkali-Metal-Depleted Vanadium-Based Prussian Blue Analogue Cathodes for Aqueous Zinc-Ion Batteries

Yingqiao Wang [abc], Yu Liu [abc], Danni Liang [abc] , Fan Liu [abc], Jian Huang [abc], Ming Chen[*ac], Wenzhuo Deng[*ac] and Chuan-Fu Sun [*ac]

[1] *State Key Laboratory of Structural Chemistry, Fujian Institute of Research on the Structure of Matter, Chinese Academy of Sciences, Fuzhou, Fujian, 350002, P. R. China*

[2] *College of Chemistry and Materials Science, Fujian Normal University, Fuzhou, Fujian 350007, China*

[3] *Fujian College, University of Chinese Academy of Sciences, Fuzhou, Fujian, 350002, P.R. China.*

Corresponding Authors:

Pro. Chuanfu Sun (email: cfsun@fjirsm. ac. cn)

Dr. Wenzhuo Deng (email: wzdeng@fjirsm.ac.cn)

Dr. Ming Chen (email: chenming@fjirsm.ac.cn)

Table of Contents

Experimental reagents

All the materials and solvents were purchased from commercial sources without further purification. Potassium ferricyanide ($K_3Fe(CN)_6$) and Vanadyl sulfate hydrate ($VOSO_4 \cdot xH_2O$) was purchased from Macklin Biochemical Co., Ltd. (Shanghai, China). Sulfuric Acid (H_2SO_4) was purchased from Sinopharm Group Co., Ltd (Shanghai, China).

Material Synthesis

$K_{0.0068}V_{1.64}O_2Fe(CN)_6 \cdot 4.2H_2O$ was synthesized via a coprecipitation method. First, 2.5 mmol of $K_3Fe(CN)_6$ was dissolved in 100 mL of deionized water and stirred at 750 rpm to obtain a clear yellow solution (solution A). Separately, 3.75 mmol of $VOSO_4 \cdot xH_2O$ was dissolved in 100 mL of 5 M H_2SO_4 to facilitate the removal of K^+ ions. Acid concentration was optimized to avoid framework collapse. After stirring for 5 min and ultrasonication for 10 min, the resulting blue suspension (solution B) was further stirred for 30 min to ensure homogeneity.

Solution B was then slowly added dropwise to solution A under continuous stirring, leading to the formation of a dark green suspension. After stirring for an additional 30 min, the mixture was allowed to stand for 2.5 h. The precipitate was collected by centrifugation, washed three times with deionized water, and dried under vacuum at 40 °C for 12 h. The dried product was ground into fine powder and repeatedly washed until the supernatant became colorless. Finally, the sample was dried at 80 °C under vacuum for 12 h to obtain the VFe powder.

Material Characterization

The phase structures of the as-prepared VFe samples and electrode materials at different electrochemical states were characterized by X-ray diffraction (XRD, Ultima IV, Rigaku). Pristine VFe powders were directly mounted on the sample holder for analysis. For electrochemical-state-dependent measurements, Zn||VFe cells were charged and discharged at a current density of 50 mA g^{-1} to designated cutoff voltages, followed by cell disassembly. The harvested electrodes were thoroughly rinsed with deionized water to remove residual electrolyte and then sealed with Kapton tape to prevent air exposure during ex situ XRD measurements. Diffraction patterns were collected over a 2ϑ range of 5°–65° at a scanning rate of 0.2° min, using Cu Kα radiation with a tube voltage of 40 kV and a tube current of 40 mA.

X-ray photoelectron spectroscopy (XPS, ESCALAB 250Xi, Thermo Scientific Instrument) was employed to investigate the elemental composition and valence state evolution of VFe electrodes at different charge–discharge states. Prior to testing, the electrodes were extracted from cycled batteries and rinsed with deionized water. The morphology and particle size of the VFe samples were examined using field-emission scanning electron microscopy

(SEM, Phenom LE) and transmission electron microscopy (TEM, Tecnai F20). Elemental distribution and quantitative composition were determined by energy-dispersive spectroscopy (EDS) and Inductively coupled plasma-Mass Spectrometry (ICP-MS, Agilent 7700x). Thermogravimetric analysis (TGA, STA 449F3, Netzsch) was conducted at a heating rate of 10 °C min^{-1} under Ar flow to evaluate the thermal stability and water content of the VFe material.

Electrochemical Characterization

CR2032-type coin cells were assembled to evaluate the electrochemical performance of the VFe cathode. The cells consisted of a Zn foil anode (14 mm diameter), 4 M $Zn(CF_3SO_2)_2$ aqueous electrolyte, a composite separator composed of Whatman glass fiber and NKK cellulose membranes(TF4050), and a VFe-based cathode.

The VFe cathode was fabricated by mixing VFe active material, carbon black, and polyvinylidene fluoride (PVDF, 5 wt%) in a mass ratio of 7:2:1 to form a homogeneous slurry. The slurry was uniformly coated onto titanium mesh current collectors (200 mesh, 10 mm diameter). The mass loading of active material was maintained at approximately 1-2 mg cm^{-2}. The coated electrodes were dried under vacuum at 80 ℃ for 12 h before cell assembly.

Electrochemical Testing

Galvanostatic charge–discharge tests were performed using a Neware battery testing system at a constant temperature of 28 °C within a voltage window of 0.2–1.95 V. Cyclic voltammetry (CV) and electrochemical impedance spectroscopy (EIS) measurements were conducted on a CHI600E electrochemical workstation. CV tests were carried out at scan rates ranging from 0.1 to 1 mV s^{-1}. EIS frequency range is 10^6 Hz to 0.1 Hz

The galvanostatic intermittent titration technique (GITT) was applied using a LANHE CT2001 system to evaluate Zn^{2+} diffusion kinetics. A current pulse of 50 mA g^{-1} was applied for 30 min, followed by a relaxation period of 2 h, and the process was repeated until the voltage reached the preset limits. Prior to GITT measurements, the cells were activated by three galvanostatic cycles at 50 mA g^{-1}. The Zn^{2+} diffusion coefficient was calculated based on the standard GITT equation.

$$D_{Zn^{2+}} = \frac{4}{\tau\pi}\left(\frac{n_M V_M}{S}\right)^2\left(\frac{\Delta E_s}{\Delta E_t}\right)^2$$

Here, τ is the duration of the constant current pulse; V_M and n_M are the molar volume and amount of active material, respectively; S denotes the effective contact area, approximated here by the geometric area. ΔE_s and ΔE_t correspond to the changes in steady-state and overall cell voltage, respectively, observed during a single-step GITT pulse.

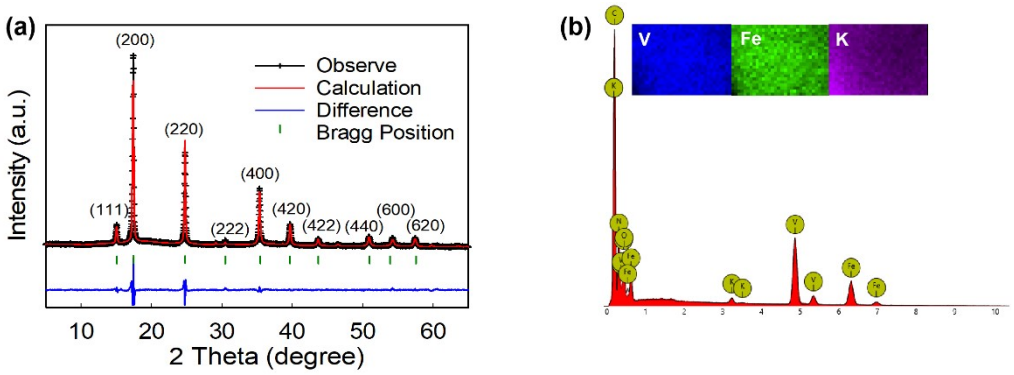

Fig. S1 (a) XRD and Rietveld refinement of VFe MPs. (b) EDS spectrum and elemental distribution of VFe.

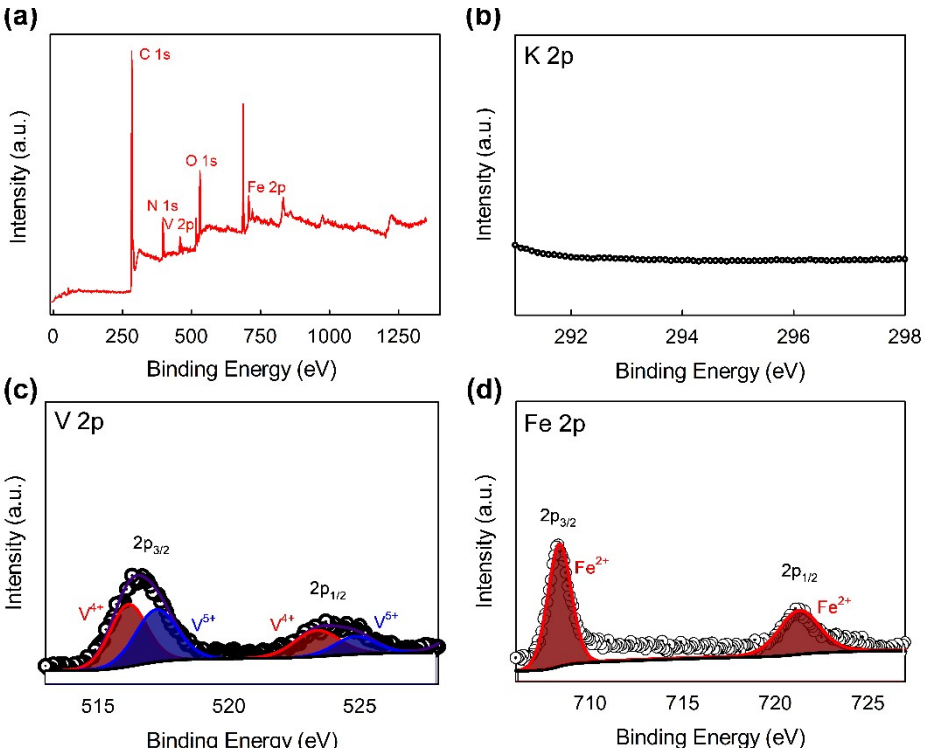

Fig. S2 XPS spectra of VFe.

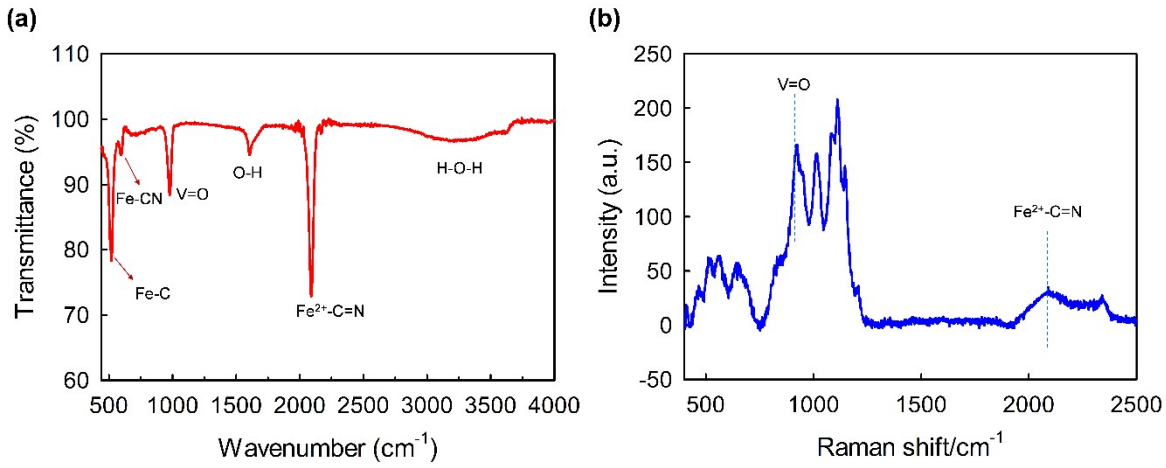

Fig. S3 (a) FT-IR spectrum and (b) Raman spectrum of VFe

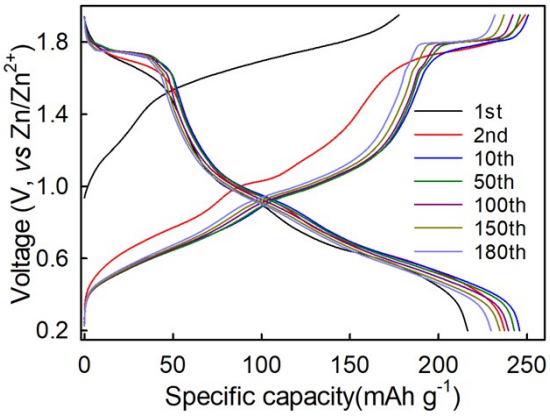

Fig. S4 Galvanostatic charge/discharge voltage profiles at 50 mA g^{-1}.

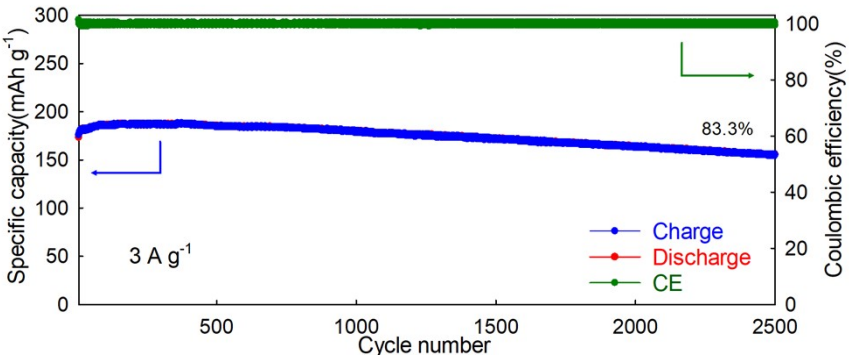

Fig. S5 Galvanostatic cycling stability at 3 A g^{-1}.

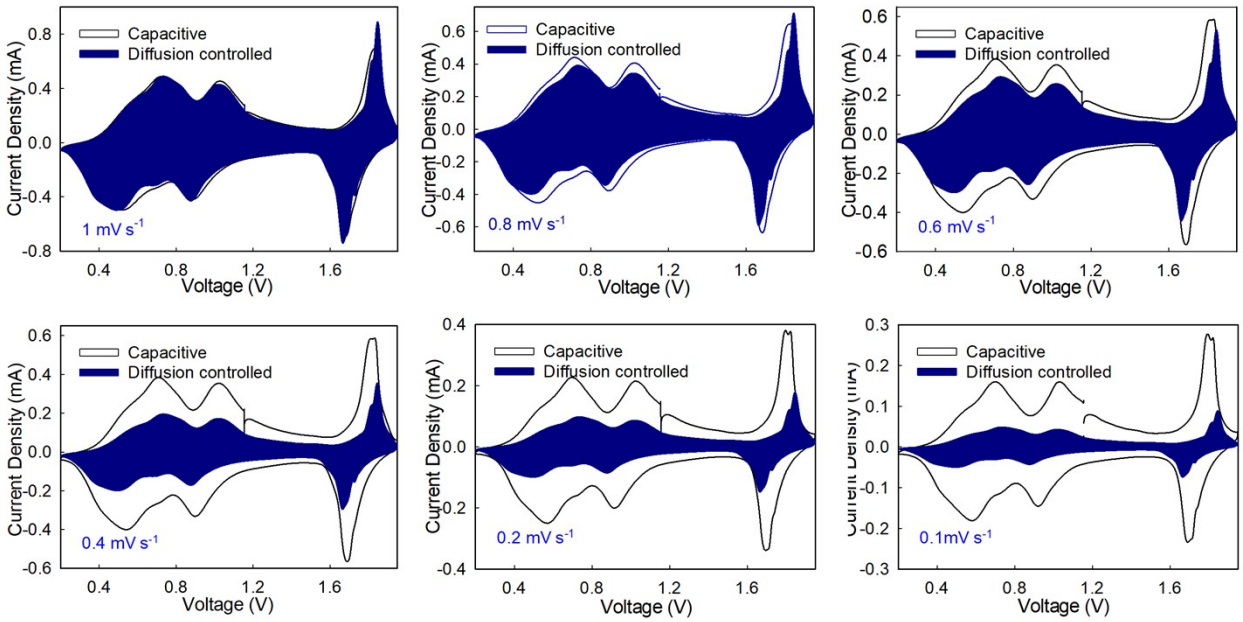

Fig. S6 Separation of the capacitive and diffusion controlled current contribution at 1 mV s^{-1}, 0.8 mV s^{-1}, 0.6 mV s^{-1}, 0.4 mV s^{-1}, 0.2 mV s^{-1} and 0.1mV s^{-1}.

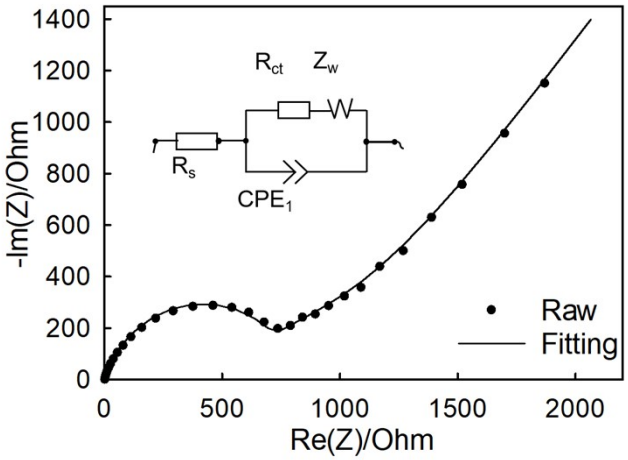

Fig. S7. Nyquist plot of electrochemical cell in open-circuit state.

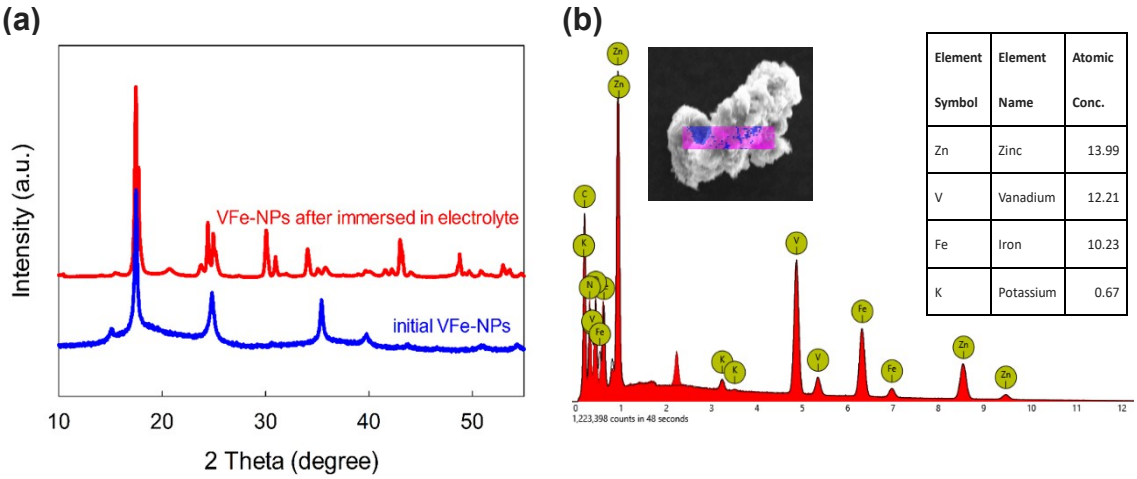

Element Symbol	Element Name	Atomic Conc.
Zn	Zinc	13.99
V	Vanadium	12.21
Fe	Iron	10.23
K	Potassium	0.67

Fig. S8. (a) XRD patterns of VFe-NPs before and after 24 h immersion in the electrolyte. (b) EDS of VFe-NPs after 24 h immersion in the electrolyte.

Table S1. ICP-MS Elemental Contents of VFe.

Element	***K***	***V***	***Fe***
Mass percentage (%)	*0.0074*	*17.89*	*10.87*
Molar ratio	*0.0068*	*1.64*	*1*

Table S2. Rate Performance of different Vanadium-Based Cathode Materials in aqueous zinc-ion batteries

Ref.	*Cathode*	*Rate performance*
	This work	*Specific capacities of 232.4, 227.5, 221.6, 215.8, 209.8, 202.9, 197.6, 191.8, 180.1, 172.3, 166.7, 158.9 and 154.2 mAh g^{-1} at current densities of 0.1, 0.2, 0.3, 0.5, 1, 2, 3, 5, 8, 10, 12 and 15 A g^{-1}, respectively*
[1]	*$Na_5V_{12}O_{32}$*	*Specific capacities of 290.6, 244.5, 199, 121.3 and 59.7 mAh g^{-1} at current densities of 0.3, 0.5, 1, 2 and 5 A g^{-1}, respectively*
[2]	*$ZnV_6O_{16}{\cdot}8H_2O$*	*Specific capacities of 400, 355, 328, 295, 238, 198 and 167 mAh g^{-1} at current densities of 0.3, 0.6, 1, 2, 5, 10 and 15 A g^{-1}, respectively*
[3]	*$Zn_{0.3}V_2O_5{\cdot}1.5H_2O$*	*Specific capacities of 426, 400, 389, 369, 335 and 265 mAh g^{-1} at current densities of 0.2, 0.5, 1, 2, 5 and 10 A g^{-1}, respectively*
[4]	*$KV_5O_{13}{\cdot}nH_2O$*	*Specific capacities of 444, 428, 411, 388, 370, 357, 336, 323 and 313 mAh g^{-1} at current densities of 0.2, 0.5, 1, 2, 3, 4, 6, 8 and 10 A g^{-1}, respectively*
[5]	*$Li_xV_2O_5{\cdot}nH_2O$*	*Specific capacities of 470, 386, 316, 236, 190 and 170 mAh g^{-1} at current densities of 0.5, 1, 2, 5, 8 and 10 A g^{-1}, respectively*
[6]	*VHCF*	*Specific capacities of 179, 162, 146, 132 and 122 mAh g^{-1} at current densities of 1, 2, 3, 4 and 5 A g^{-1}, respectively*
[7]	*KVHCF*	*Specific capacities of 180, 179, 174, 168, 161, 136, and 116 mAh g^{-1} at current densities of 0.4, 1, 22, 3, 4, 6, and 8 A g^{-1}, respectively*
[8]	*(CoNiHCF)/CNTs*	*Specific capacities of 135.4, 94.9, 72.9, 54.1, 44.1, and 35.1 mAh g^{-1} at current densities of 0.05, 0.1, 0.2, 0.5, 1, and 3 A g^{-1}, respectively*
[9]	*(Mn–Co-PBA)@CF*	*Specific capacities of 138, 128, 123, 111 and 95 mAh g^{-1} at current densities of 0.1, 0.2, 0.3, 0.5, and 1 A g^{-1}, respectively*
[10]	*GSAF@KVO-HCF*	*Specific capacities of 162, 157, 152, 144, 138, 129 and 119 mAh g^{-1} at current densities of 0.1, 0.2, 0.4, 0.8, 1.6, 2, and 3 A g^{-1}, respectively*
[11]	*Mn@FeHCF*	*Specific capacities of 163.5, 157.5, 149.5, 145.6, 140.2, 132.7,125.4,117.3, and 109.9 mAh g^{-1} at current densities of 0.1, 0.2, 0.5, 0.7, 1, 1.5, 2, 2.5, and 3 A g^{-1}, respectively*
[12]	*MgVOH/PANI*	*Specific capacities of 332, 267, 216 and 178 mAh g^{-1} at current densities of 0.2, 0.5, 1 and 2 A g^{-1}, respectively*
[13]	*Co-δ-MnO_2*	*Specific capacities of 408.9, 402.6, 368.2, 312.8, 263.2, and 232.7 mAh g^{-1} at current densities of 0.1, 0.2, 0.5, 1, 2, and 3 A g^{-1}, respectively*

Table S3 Variations in elemental content of VFe at Each stage detected by EDS testing

State	***A***	***B***	***C***	***D***	***E***
Zn (%)	*23.83*	*11.37*	*13.32*	*5.94*	*32.92*
Fe (%)	*1.58*	*2.44*	*1.14*	*0.25*	*1.65*
V (%)	*2.59*	*3.59*	*9.16*	*4.69*	*3.92*

References

[1] GUO X, FANG G, ZHANG W, et al. Mechanistic insights of Zn^{2+} storage in sodium vanadates [J]. Advanced Energy Materials, 2018, 8(27): 1801819.

[2] ZHANG Y, WAN F, HUANG S, et al. A chemically self-charging aqueous zinc-ion battery [J]. Nature communications, 2020, 11(1): 2199.

[3] WANG L, HUANG K-W, CHEN J, et al. Ultralong cycle stability of aqueous zinc-ion batteries with zinc vanadium oxide cathodes [J]. Science advances, 2019, 5(10): eaax4279.

[4] QIU N, YANG Z, XUE R, et al. Toward a high-performance aqueous zinc ion battery: potassium vanadate nanobelts and carbon enhanced zinc foil [J]. Nano Letters, 2021, 21(7): 2738–2744.

[5] YANG Y, TANG Y, FANG G, et al. Li^+ intercalated $V_2O_5 \cdot nH_2O$ with enlarged layer spacing and fast ion diffusion as an aqueous zinc-ion battery cathode [J]. Energy & Environmental Science, 2018, 11(11): 3157–3162.

[6] ZHANG Y, WANG Y, LU L, et al. Vanadium hexacyanoferrate with two redox active sites as cathode material for aqueous Zn-ion batteries [J]. Journal of Power Sources, 2021, 484: 229263.

[7] WANG F, LI Y, ZHU W, et al. Zn-ion batteries: boosting the rate capability and low-temperature performance by combining structure and morphology engineering [J]. ACS Applied Materials & Interfaces, 2021, 13(29): 34468–34476.

[8] CAO J, XUE Y, JI Z, et al. CoNi hexacyanoferrate nanoparticles anchored on carbon nanotubes as superior cathode materials for rechargeable aqueous zinc-ion batteries [J]. Journal of Energy Storage, 2024, 86: 111413.

[9] REDDY B P, PRASAD P R, MALLIKARJUNA K, et al. Mn–Co Prussian blue analogue cubic frames for efficient aqueous Zn ion batteries [J]. Microporous and Mesoporous Materials, 2023, 362: 112793.

[10] MA H, CHEN R, LIU B, et al. Synthesis of ultrasmall vanadium ferricyanide nanocrystallines with the aidance of graphene self-assembled fibers towards reinforced zinc storage performance [J]. Chemical Engineering Journal, 2024, 489: 151112.

[11] YANG G, LIANG Z, LI Q, et al. Epitaxial core–shell MnFe prussian blue cathode for highly stable aqueous zinc batteries [J]. ACS Energy Letters, 2023, 8(10): 4085–4095.

[12] HU L, SUN Q, CAI H, et al. Metal ions and organic molecule co-intercalated vanadium oxide cathode for high-performance zinc-ion batteries [J]. Materials Science in Semiconductor Processing, 2024, 177: 108358.

[13] YANG S, LI F, FU P, et al. Room temperature synthesis of the Co-doped δ-MnO_2 cathode for high-performance zinc-ion batteries [J]. Journal of Power Sources, 2024, 611: 234767.